Solution Processed Fabrication of Se-Te Alloy Thin Films for Application in PV Devices

Swapnil D. Deshmukh,[1] Caleb K. Miskin,[1] Apurva A. Pradhan,[1] Kim Kisslinger,[2] Rakesh Agrawal[1]*

[1]Davidson School of Chemical Engineering, Purdue University, West Lafayette, IN 47907, USA
[2]Center for Functional Nanomaterials, Brookhaven National Laboratory, Upton, NY 11973, USA

Abstract

In this work, we report the first-ever fabrication of solution-processed Se-Te alloy thin films for photovoltaic applications using an amine-thiol solvent system. By controlling the relative quantity of Se and Te in ethylenediamine-ethanethiol (EN-ET) solution mixture, films with different Se:Te ratios were fabricated at temperatures as low as 200 °C with phase pure material synthesis and uniform homogenous alloying. These composition variations then successfully demonstrated bandgap variation from 1.80 eV for pure Se to 1.18 eV for a film with 60% Se and 40% Te that closely matches the theoretical values calculated from Vegard's law for these materials. Using the evaporation process, the isolation of chalcogen complexes from the EN-ET solution was performed which was followed by the addition of foreign solvents like dimethyl sulfoxide, dimethyl formamide, and ethanolamine which enabled the fabrication of better quality films using the spin coating process minimizing the porosity and increasing the uniformity of the film. A preliminary device fabricated from these films showed diode characteristics with encouraging photovoltaic performance (power conversion efficiency of 1.11%) that demands further optimization with film fabrication, selection of device architecture, and detailed defect analysis for this material.

Introduction

Selenium is the world's first material that was used in solid-state photovoltaic devices. The increase in selenium conductivity after the illumination of light led to its application in solar cells. However, for a long time, the device fabricated from selenium absorber remained at the highest efficiency of 5% which was achieved in 1984.[1] Due to the rapid increase in efficiency of its competitor, Si, more research was focused on Si-based solar cells which currently has a record high efficiency above 26%.[2] Although Se did not get much attention as individual photovoltaic material in past years, it has been part of some high-efficiency metal chalcogenide solar cell materials[3] like $Cu(In,Ga)Se_2$,[4] $Cu_2ZnSnSe_4$,[5] and Cd(Se,Te).[6] Recently few research groups have again started working on pure Se-based photovoltaic devices.[7–14] The reason for this can be attributed to its properties and ease of fabrication. Se has a high absorption coefficient and can be fabricated at temperatures below its melting point which is 220 °C making it a material suitable for scalable deposition. Its bandgap in the trigonal crystal structure is between 1.75-2 eV which could act as a high bandgap device in tandem device architectures. Currently, the new research especially in the field of device architecture has led the Se solar cell efficiency improvement to 6.51% with absorber thickness of only 100 nm.[9] This result promises great potential for improvements in Se photovoltaic devices.

While Se is a promising material for photovoltaic application, its high bandgap isn't necessarily in the range which is considered ideal (1-1.5 eV) for high-efficiency single-junction solar cells according to Shockley–Queisser limit. So, to reduce its bandgap, alloying with the same group element as tellurium which has a bandgap of 0.35 eV is desired. Such alloying with the formation of amorphous material has shown to decrease the bandgap of Se with increasing Te concentration.[15–17] While some reports also suggest similar behavior in the crystalline alloys, a recent report on Se-Te alloy thin films showed non-linear dependence of composition on Se-Te alloy bandgap.[18] This same report along with some other reports demonstrated a solar cell fabrication with Se-Te alloy thin films.[18,19] Although these attempts for fabrication of Se-Te alloy solar cells have yielded lower efficiency than Te-free, pure Se solar cells, it does show an increase in current collection with decreasing bandgap of the material. More work on the electron and hole transport layers could further help improve these efficiencies for Se-Te alloy solar cells.

Currently the fabrication of Se or Se-Te alloy solar cells has primarily utilized vacuum-based thermal evaporation processes. So, one still has scope to develop solution-based routes that allow for its fabrication at not only lower temperatures but also at atmospheric pressures which facilitates scale up for high throughput, low cost manufacturing. One such attempt for fabricating Se solar cells using solution processing was reported with a hydrazine solvent system.[8] While it did produce solar cells with efficiency above 3%, it didn't show alloying with Te and more importantly, it used a solvent that is extremely toxic, carcinogenic, and explosive.

In this work, we have utilized a relatively safer amine-thiol solvent system and its ability to dissolve pure chalcogens to fabricate the first-ever direct deposited solution-processed thin film of Se-Te alloy. Using different relative ratios of Se and Te in ethylenediamine-ethanethiol solution, films with different compositions were fabricated that showed a gradual decrease in optical bandgap with increasing tellurium concentration. Utilizing our previously discovered understanding of the complexes formed in these solutions, we modified the solvent selection for the film fabrication that resulted in improved microstructural film quality. This optimized film fabrication was then incorporated in a device

architecture to demonstrate the photovoltaic nature of the alloyed Se-Te films. While the preliminary efficiency of 1.11% was achieved for a film with 30% Te and 70% Se, more work on film optimization, band alignments and selection of electron transport layer (ETL) and hole transport layer (HTL) should help improve this performance.

Experimental Section

Materials

Se (100 mesh, 99.99%), Te (30 mesh, 99.997%), Titanium (IV) isopropoxide (99.999%), Ethylenediamine (EN, 99%), Ethanethiol (ET, 97%), Dimethyl sulfoxide (DMSO, 99.9%), Dimethyl formamide (DMF, 99.8%), Ethanolamine (EA, 99%), $N^2,N^2,N^{2'},N^{2'},N^7,N^7,N^{7'},N^{7'}$-octakis(4-methoxyphenyl)-9,9′-spirobi[9H-fluorene]-2,2′,7,7′-tetramine (Spiro-OMeTAD, 99%) were purchased from Sigma-Aldrich. All chemicals were used as received.

Ink Formulation

Se and Te were dissolved in ethylenediamine (EN) and ethanethiol (ET) solution with EN:ET volume ratio of 4:1. Four different solutions were prepared for $Se_{1-x}Te_x$ with x = 0, 0.1, 0.2, 0.3. These dissolutions were performed at room temperature in a nitrogen-filled glovebox under constant stirring at 300 rpm. While Te-free solutions were dissolved completely at 4 M Se concentration within 15 min, Te containing inks took around 2-4 hours depending on Te concentration for complete dissolution at total chalcogen concentration of 4 M. Due to higher chalcogen concentrations all inks appeared dark red. These inks were then used for film fabrication without further filtration. For solvent engineering, the above-prepared inks were subjected to vacuum at room temperature to remove excess amine and thiol from the solution. This was achieved on a schlenkline using an apparatus containing a single neck 15 ml flask and a condenser. Although the condenser was attached to the assembly, no cooling water was flowing through the condenser during the evaporation process. Around 4 ml of ink was transferred to a flask and then it was exposed to 200 mtorr of vacuum for 15 min under constant stirring of 100 rpm. During the evaporation process, the flask was submerged into room temperature water to prevent the ink from cooling. At the end of 15 min evaporation process, a dark red color viscous complex was obtained which was then sealed under vacuum and transferred to the glovebox for new ink formulations. The complex was redissolved in various solvents to again get an approximate chalcogen concentration of 4 M and then used for film fabrication.

Ink for dense TiO_2 layer (TTIP solution) was prepared by mixing 5 mL ethanol, 35 µL HCl 2M, and 370 µL titanium (IV) isopropoxide. Ink for meso TiO_2 layer was prepared by diluting TiO_2 paste in ethanol. Ink for hole transport layer was prepared by mixing 80 mg of Spiro-OMeTAD, 30 µl bis(trifluoromethane) sulfonimide lithium salt stock solution (500 mg Li-TFSI in 1 ml acetonitrile), 30 µl 4-tert-butylpyridine (TBP), and 1 ml chlorobenzene solvent.

Thin Film and PV Device Fabrication

Dense TiO_2 layer was deposited on the FTO coated soda-lime glass (13 ohm/sq) using spin coating technique (2000 rpm for 30 s) using TTIP solution and was annealed at 500 °C in the air for 1 hour. A layer of meso TiO_2 was deposited on top of it from a solution of TiO_2 nanoparticles in ethanol. For Se-Te film deposition, Se-Te ink (4 M) was spin coated at around 3000 rpm for 30 sec on TiO_2 films followed by annealing at 120 °C for 5 min in a nitrogen atmosphere. This resulted in a red-colored film which was then annealed at 200 °C for 2 – 3 min. One to two layers of these inks were deposited in order to get desired thickness depending on the experiment. After the deposition of Se-Te alloy film, 1 layer of Spiro-OMeTAD solution was deposited using spin coating at 2000 rpm for 30 s as a hole transport layer which was allowed to dry at room temperature in a nitrogen atmosphere. Finally, 200 nm of Au was deposited as back contact to finish the device using thermal evaporation, and cells with an area of ~0.1 cm^2 were mechanically scribed from this film. Films for UV-vis absorption spectroscopy were fabricated on Al_2O_3 coated SLG substrates using spin coating at 3000 rpm for 30 sec with inks having a total chalcogen concentration of 1 M instead of 4 M to obtain thin semi-transparent films.

Characterization

X-ray diffractograms (XRD) were obtained using a Rigaku Smart Lab diffractometer in Bragg-Brentano mode, using a Cu Kα (λ = 1.5406 Å) source operating at 40kV/44mA. Scanning electron microscopy (SEM) images were collected using an FEI Quanta 3D SEM at an accelerating voltage of 10 kV, 4.0 spot size, and a working distance of ~10 mm using the ETD (Everhart Thornley Detector). Samples for TEM analysis were prepared by cutting a cross-section of particles using Focused Ion Beam (FIB) in an FEI Helios SEM. STEM-EDS data were collected on Talos 200X TEM containing four silicon drift detectors. Raman and PL spectra were collected on Horiba/Jobin-Yvon HR800 microscope with an excitation laser wavelength of 632.8 nm. The bulk film composition was analyzed using a Fisher XAN 250 X-ray fluorescence (XRF) instrument. Absorption data was collected using LAMBDA 950 UV-vis dual-beam spectrometer in transmission mode. The transmission spectra (% transmittance) were then converted into absorbance using relation A=2-log(T%). The J-V characteristics were measured with a four-point probe station using Keithley 2400 series source meter while the illumination was provided by a Newport Oriel solar simulator with an AM1.5 filter set and calibrated to 1 sun intensity using a Si reference cell certified by NIST.

Result and Discussion

Fabrication of Se-Te alloy films

The amine-thiol solvent system has been used in the fabrication of a variety of metal chalcogenide (sulfide, selenide, and telluride) semiconducting materials.[20–25] This solvent system has been studied extensively for its chemistry of dissolving a variety of precursors at room temperature suitable for different applications.[26–28] Se and Te are two such precursors that are known to dissolve in EN-ET solution at concentrations as high as 6 M for Se and 0.6 M for Te. The solubility limit for Te is also

known to increase beyond 0.6 M when it is co-dissolved with Se allowing for the preparation of high concentration inks for film fabrication.[26] First, to verify the possible alloying of Se and Te in the film from amine-thiol solution, four Se-Te inks with Te/(Se+Te) ratio of 0, 0.1, 0.2, and 0.3 were prepared in EN-ET solution at an overall chalcogen concentration of 4 M. These inks were then used to spin coat a layer of Se-Te material to obtain a thin film morphology. However, the EN-ET solvent system does not wet the soda-lime glass properly which limits the uniform film fabrication process with this solvent. To resolve this issue, Al_2O_3 nanoparticles suspended in alcohol were used to create a thin layer on soda-lime glass which made the surface suitable for spin coating of EN-ET inks. This spin coating was performed at 3000 rpm and the films obtained from it were annealed at 120 °C for 5 min in an inert nitrogen atmosphere to remove excess EN and ET from the film. This drying step resulted in a red-colored film which was then converted into gray/black color film with annealing at 200 °C for 2 min. These films were then analyzed in XRD for identifying the crystal structure and extent of alloying in the material. As can be seen from Figure 1a, all films produced crystalline trigonal phase with peak positions moving towards lower diffraction angle for films with increasing Te content. Peaks corresponding to elemental Se and Te are missing from alloyed films which confirms uniform and homogeneous alloying between Se and Te in the thin-film architecture. When these films were analyzed under Raman spectroscopy, a transition of Se-Se bond (234 cm^{-1}) in trigonal Se structure towards the Se-Te bond was observed through the detection of peaks at frequencies below 200 cm^{-1} (Figure 1b).[29] While it is already known that amorphous Te is highly unstable and is readily converted to crystalline material at room temperature, the absence of Raman peak at 250 cm^{-1} (a-Se) and 157 cm^{-1} (a-Te) further supports the absence of any amorphous elemental Se or Te in the film.[30,31] Although these films were fabricated with inks containing Te/(Se+Te) ratio of 0, 0.1, 0.2, and 0.3, after fabricating the films, XRF suggested Te/(Se+Te) ratio of 0, 0.15, 0.3, and 0.4 respectively in these films. This increase in the relative quantity of Te in the films can be attributed to some loss of Se during annealing at 200 °C.

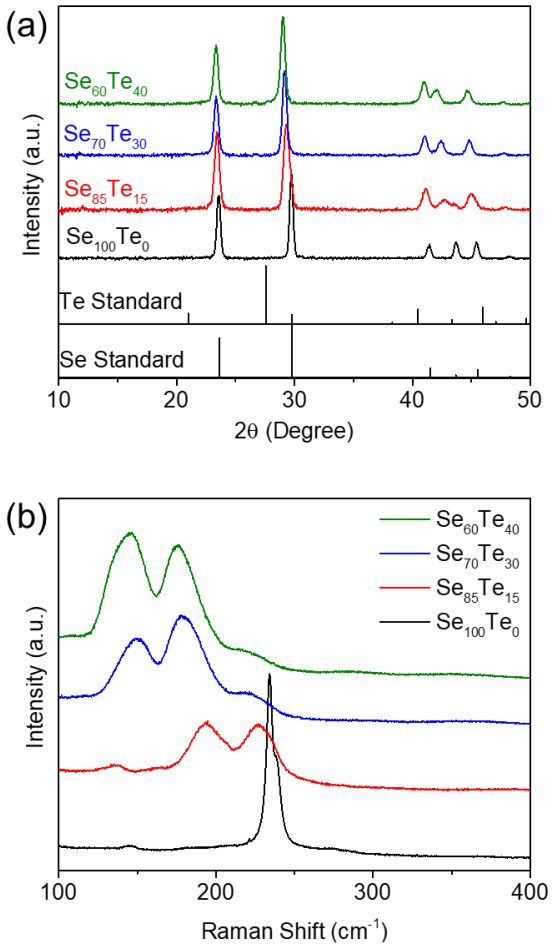

Figure 1. (a) XRD (Se ICSD collection code #53801, Te ICSD collection code #96502) and (b) Raman data of $Se_{1-x}Te_x$ alloy thin films fabricated from Se-Te-EN-ET solution

While XRD and Raman spectroscopy confirmed the microscopic alloying of Se and Te in thin films, its effect on optical property, i.e. absorption was studied using UV-Vis absorption spectroscopy. Absorption data collected on these films showed increasing absorption at longer wavelengths for films containing a higher quantity of Te confirming the reduction in the optical bandgap of Se with Te alloying. The exact value of the bandgap was obtained from this data by converting it into a tauc plot as shown in Figure 2a. This plot suggests the bandgap of 1.85 eV, 1.64 eV, 1.35 eV, and 1.18 eV for Se, $Se_{85}Te_{15}$, $Se_{70}Te_{30}$, and $Se_{60}Te_{40}$ films. These values of bandgap surprisingly fit the linear correlation proposed based on Vegard's law which predicts bandgap values of 1.80 eV, 1.58 eV, 1.36 eV, and 1.22 eV. This is a contradictory result to the one recently reported by Hadar et al.,[18] where a non-linear correlation was observed for Se-Te alloy films that were fabricated using the thermal evaporation technique. This report predicted the bandgap values of 1.80 eV, 1.44 eV, 1.13 eV, and 0.96 eV for the above 4 compositions which are lower than the one observed here. The reason for this difference isn't completely clear, but it could be associated with the film deposition technique. As during thermal evaporation, due to the difference in vapor pressure of Se and Te material, some

amount of non-uniformity could be generated in the film which could allow for absorption of lower energy photons if some region in the film is Se poor than the targeted value. If this indeed is the reason for bandgap differences, then solution processing provides superiority in film fabrication by avoiding such non-uniformities by ensuring uniform mixing of Se and Te on a molecular level.

Another feature was observed in tauc plot especially for films with no Te and 15% Te. These spectra show the change in curvature at higher energies which implies the presence of material with a higher bandgap. This higher energy transition observed here can be attributed to quantum confinement behavior. It has been reported in the literature for Se quantum dots to have bandgaps even above 3 eV depending on the size of the quantum dots.[32] As we are using solution chemistry to make these films and especially for UV-vis the film thickness is around 50-100 nm, it is possible to have some nanoparticle formation which would have a higher bandgap than the bulk material. Similar reasoning applies to the films containing Te where possible quantum confinement could be a reason for the appearance of secondary higher bandgap transition. However, the bulk bandgap obtained from tauc plot will be more relevant for its application in solar cell architecture.

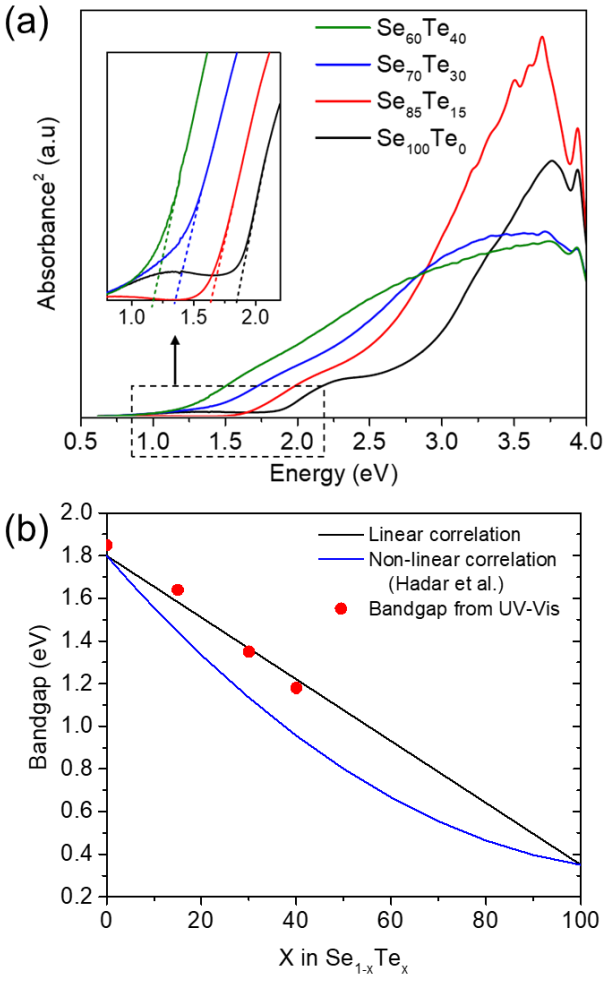

Figure 2. (a) Complete Tauc plot with a zoomed version (insert) from data collected using UV-vis absorption spectroscopy for $Se_{1-x}Te_x$ alloy thin films (b) Bandgap calculated from tauc plot as a function of composition along with recently proposed non-linear correlation for Se-Te alloy thin films fabricated from the thermal evaporation process[18]

Solvent Engineering

After successful fabrication of Se-Te alloy thin films with controlled bandgap from the amine-thiol solution route, the morphology of the films being produced was studied using SEM analysis. As a bandgap of 1.35 eV appears to be in the ideal range for high-efficiency single-junction devices, the film microstructure optimization was performed on films fabricated from the ink containing Te/(Se+Te) ratio of 0.2. This film optimization was performed on films fabricated on FTO substrate that is coated with both dense and meso TiO_2 layers. Traditionally, to get thicker films for any material, multiple layers of the ink are coated and annealed. This allows for the removal of solvent from one layer with the formation of the desired material in thin-film architecture. As the material formed after annealing is generally insoluble in the precursor ink (e.g. during fabrication of $CuInS_2$ films from the amine-thiol solvent system, while the ink contains copper, indium, and sulfur precursors, the $CuInS_2$ material formed after annealing is insoluble in amine-thiol solution) coating another layer on top of it is a feasible option to increase the thickness of the film. However, in the case of fabrication of Se-Te alloy thin film, no new material is formed and the coated material i.e. Se and Te are still soluble in the solvent used for the next layer which is the EN-ET mixture. So, to achieve larger thicknesses, one needs to saturate the ink such that it won't allow for the dissolution of coated material during the deposition of a consecutive layer. This was achieved by manipulating the solvents used for the dissolution. It is already known that both EN and ET are necessary to dissolve Se and Te in the solution and the absence of one could limit their solubility. So, after preparing Se-Te ink in EN-ET solvent, the solution was exposed to vacuum at room temperature to remove excess/unreacted EN and ET from the solution. This resulted in the isolation of alkylammonium selenium and tellurium complexes. While pure Se and Te are insoluble in EN alone, these Se-Te complexes were found to be soluble in just EN without any addition of ET allowing for the formulation of ET free Se-Te complex ink that can be used for multiple layer deposition. The importance of creating such ink was evident from the quality of the films produced from it. As can be seen from SEM images in Figure 3, 2 layers of EN-ET ink resulted in a film with relatively higher porosity while the one fabricated with isolated complexes redissolved in EN solvent resulted in much lower porosity.

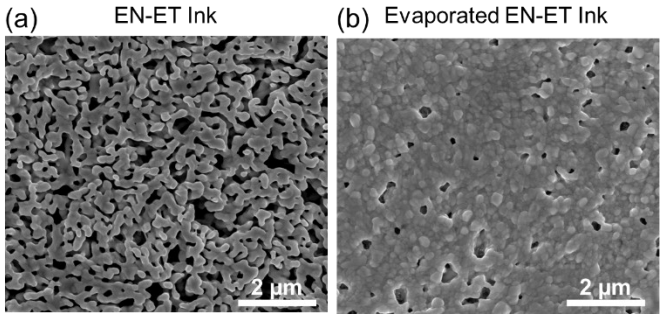

Figure 3. SEM images for spin coated 2 layer Se-Te alloy films fabricated from (a) as prepared Se-Te ink in EN-ET solvent and (b) ink formulated by isolating Se-Te complex from EN-ET solution and redissolving it in only EN solvent

While the use of isolated complexes in EN resulted in relatively denser film morphology, it still contained few pores with a diameter up to 100 nm. Such pores could act as shunting pathways when a device is fabricated from this film. As ample literature has shown the effect of solvent engineering on film quality,[33] a similar approach was studied for Se-Te films. This was achieved by adding a foreign solvent to the ink before film fabrication. To maintain the identical chalcogen concentration in the ink, the isolated Se-Te complex was redissolved in 50:50 volume ratio of EN and some other foreign solvent like dimethyl sulfoxide (DMSO), dimethyl formamide (DMF), and ethanolamine (EA). These solvents were selected due to the difference in their boiling points (DMSO-189°C, DMF-153°C, and EA-170°C) compared to EN (116°C) and the presence of different functional groups in these molecules. Both of these parameters could alter the drying step during film annealing and can affect the film microstructure. When 2 layer films were fabricated from these modified inks, a significant difference in microstructure morphology was observed from the SEM images of these films. The DMSO-based film showed an overall larger and continuous grain structure, but it also produced relatively larger pores compared to EN-based film. On the other hand, the remaining two solvents reduced the overall porosity in the film with EA-based film being the most uniform and least porous film as can be seen in Figure 4a. While the overall microstructure of the film was influenced by the selection of solvent, the film thickness measured from XRF did not show much difference between these films. All solvents with 2 layers of coating yielded films with thickness in the range of 700-750 nm.

With EA-based film producing uniform film, another parameter for film fabrication was altered to study its effect on the quality of film microstructure. This parameter was the speed of the spin coating step. While all the previous films were fabricated with 3000 rpm, the EA ink was used to fabricate films at some lower speeds as well. As can be seen from Figure 4b, with reducing the speed of the spin coating step, larger grain sizes were obtained for the films. This result can be explained based on the increased material quantity on the film prior to annealing. With the reduction of spin coating speed by a factor of 10, the thickness of the liquid layer remaining on the substrate must be getting higher resulting in a much larger amount of Se-Te material being present on the substrate which would grow bigger grains and thicker films.

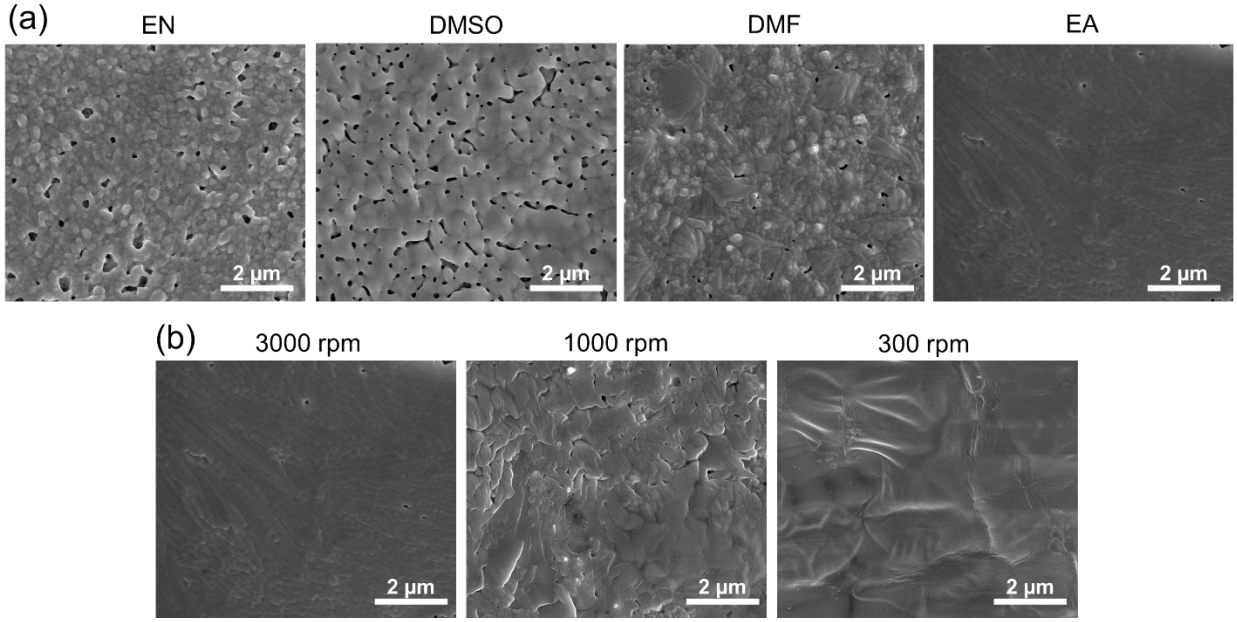

Figure 4. SEM images of Se-Te alloy thin films fabricated with (a) inks formulated using different solvent additions and (b) different spin coating speed for ink containing EA solvent

Device Fabrication

With successful control over film microstructure for Se-Te alloy films, its photovoltaic properties were studied by fabricating it into a working solar cell architecture. The device architecture used for these solar cells was adopted from previous reports on Se solar cells.[8] In order to improve the electron collection through increase contact surface area, meso TiO_2 along with dense TiO_2 was used as an electron transport layer. A Se-Te film was then coated on this meso TiO_2 layer and annealed as explained in the experimental section. To complete the device fabrication, Spiro-OMeTAD was used as a hole transport layer followed by Au as a metal back contact. Figure 5 illustrates the device architecture used for Se-Te alloy solar cell fabrication. As the meso TiO_2 layer was used in this device architecture for better charge transport, the film thickness was also kept at a minimum to avoid any losses from possible low diffusion length of the carriers. For this reason, instead of using 300 rpm speed which gives much bigger grains and thicker film, a 3000 rpm speed was used for film coating that gives the thinner film and smaller grains but still maintains a relatively smaller number of pores.

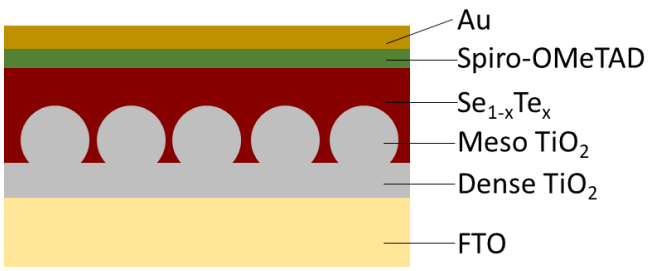

Figure 5. Schematic of $Se_{1-x}Te_x$ alloy thin-film PV device architecture

To confirm if the Se-Te solution has penetrated in the meso TiO_2 layer for better surface area contact, a focused ion beam was used to create a thin lamella from this device and was analyzed under STEM-EDS. As can be seen from STEM-EDS elemental mapping analysis in Figure 6, an area where Ti signal is observed, both Se and Te signals were also observed confirming the penetration of Se-Te ink in meso TiO_2 layer and also the uniform mixing of Se and Te in this layer.

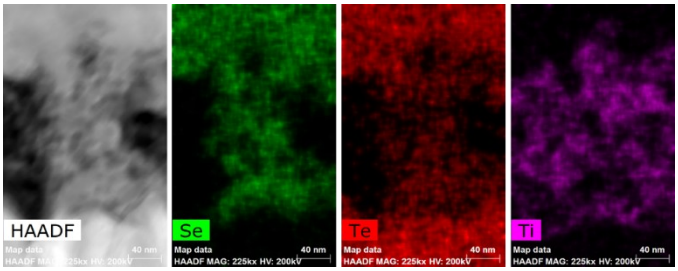

Figure 6. STEM-EDS analysis of a cross-section of Se-Te alloy thin film fabricated on TiO_2 layer confirming the presence of Se and Te in meso TiO_2 layer

With the success of Se-Te alloy film fabrication, the current-voltage analysis of the final device was performed. For this analysis, the 2.5 cm x 2.5 cm area was divided into smaller cells with each having an approximate area of 0.1 cm^2 using the mechanical scribing technique. The light was then shined from the FTO side on the device and its current-voltage response was measured. As can be seen from Figure 7, the JV response confirmed the formation of a diode. Further analysis of this data suggested power conversion efficiency of 1.11% with Jsc of 7.4 mA/cm^2, Voc of 0.41 V, and fill factor of 36.5%. Although these parameters aren't necessarily impressive, they still are promising given the initial demonstration of such device architecture using solution processing. The low Jsc can be improved with increasing absorber thickness, the low Voc can be improved with proper selection of ETL/HTL and the FF can be improved with uniform film deposition as some of the porosity in the film is likely causing shunting which can be easily identified from the slope of JV curve near short circuit condition. Along with microstructure morphology, defect analysis can also help further improve the performance of these devices.

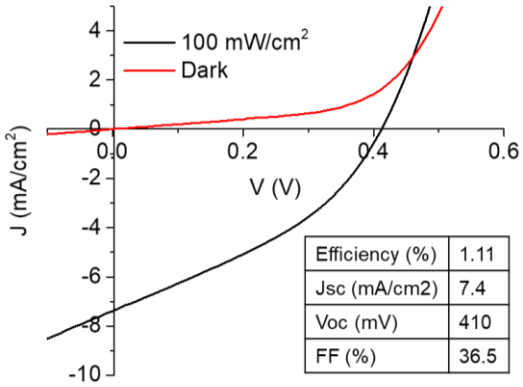

Figure 7. JV analysis of Se-Te alloy solar cell fabricated with TiO_2 as ETL and Spiro-OMeTAD as HTL

While the device fabricated from Se-Te alloy film showed diode behavior with a promise for PV, the photoluminescence data collected on films with different Te quantities showed decreasing PL intensity with increasing Te concentration. More importantly, even when the optical bandgap of material was changing with Te incorporation and a value as low as 1.18 eV was obtained with 40% Te in the film, the peak in PL responses did not show appreciable change in their position. As can be seen from Figure 8, the PL peak for Se film was observed at ~800 nm and with increasing Te concentration it showed extremely small red shift to ~830 nm for film with 40% Te (ink with 30% Te). Such behavior of PL data although seen in literature[34] isn't completely clear and needs further analysis to understand the role of Te in Se films and the viability of this material for PV application.

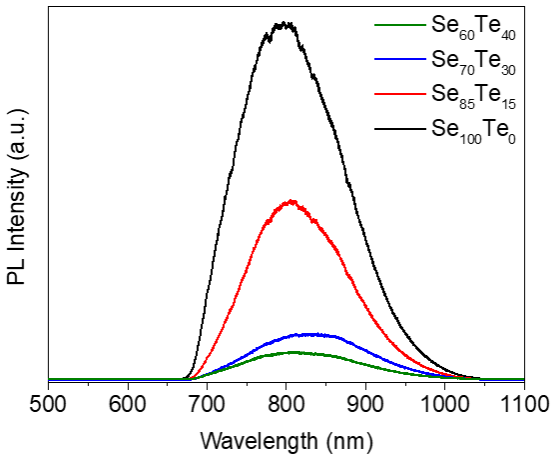

Figure 8. Photoluminescence spectra for $Se_{1-x}Te_x$ alloy thin films collected with 632.8 nm laser on Si detector

Conclusion

In conclusion, we demonstrated the fabrication of Se-Te alloy thin films using an amine-thiol solvent system making it a first-ever solution-processed Se-Te alloy thin film fabrication. XRD, Raman and STEM-EDS analysis confirmed the formation of the homogenous alloy without any presence of phase segregation. XRF of these films showed loss of Se in the annealing step giving Te rich films compared to precursor inks, while the UV-Vis absorption spectroscopy suggested a linear correlation of bandgap to the composition of the alloy. Through isolation of Se-Te complex and solvent engineering, the film quality was improved to obtain films with reduced porosity as well as larger grains. A preliminary photovoltaic device fabricated using TiO_2 as ETL and Spiro-OMeTAD as HTL confirmed the formation of a diode and yielded power conversion efficiency of 1.11% for $Se_{70}Te_{30}$ alloy. More optimization on film fabrication as well as ETL and HTL selection with detailed analysis of defects in this material promises further improvement in solar cell efficiencies.

Acknowledgment

The authors would also like to acknowledge the funding support provided by the National Science Foundation under grants 1534691-DMR (DMREF), 1735282-NRT (SFEWS), and 1855882 (INFEWS). The research was carried out in part at the Center for Functional Nanomaterials, Brookhaven National Laboratory, which is supported by the U.S. Department of Energy, Office of Basic Energy Sciences, under Contract No. DE-SC0012704.

References

1. Champness, C. H. & Chan, C. H. Related content Selenium Thin-Film Solar Cell. (1984).
2. Green, M., Dunlop, E., Hohl-Ebinger, J., Yoshita, M., Kopidakis, N. & Hao, X. Solar cell efficiency tables (version 57). *Prog. Photovoltaics Res. Appl.* **29,** 3–15 (2021).
3. Dey, T. Role of earth-abundant selenium in different types of solar cells. *J. Electr. Eng.* **72,** 132–139 (2021).
4. Nakamura, M., Yamaguchi, K., Kimoto, Y., Yasaki, Y., Kato, T. & Sugimoto, H. Cd-free Cu(In,Ga)(Se,S)$_2$ thin-film solar cell with a new world record efficacy of 23.35%. in *46th IEEE PVSC* (2019).
5. Wang, W., Winkler, M. T., Gunawan, O., Gokmen, T., Todorov, T. K., Zhu, Y. & Mitzi, D. B. Device characteristics of CZTSSe thin-film solar cells with 12.6% efficiency. *Adv. Energy Mater.* **4,** 1–5 (2014).
6. Poplawsky, J. D., Guo, W., Paudel, N., Ng, A., More, K., Leonard, D. & Yan, Y. Structural and compositional dependence of the $CdTe_xSe_{1-x}$ alloy layer photoactivity in CdTe-based solar cells. *Nat. Commun.* **7,** 1–10 (2016).
7. Wang, K., Shi, Y., Zhang, H., Xing, Y., Dong, Q. & Ma, T. Selenium as a photoabsorber for inorganic-organic hybrid solar cells. *Phys. Chem. Chem. Phys.* **16,** 23316–23319 (2014).
8. Zhu, M., Hao, F., Ma, L., Song, T. Bin, Miller, C. E., Wasielewski, M. R., Li, X. & Kanatzidis, M. G. Solution-Processed Air-Stable Mesoscopic Selenium Solar Cells. *ACS Energy Lett.* **1,** 469–473 (2016).
9. Todorov, T. K., Singh, S., Bishop, D. M., Gunawan, O., Lee, Y. S., Gershon, T. S., Brew, K. W., Antunez, P. D. & Haight, R. Ultrathin high band gap solar cells with improved efficiencies from the world's oldest photovoltaic material. *Nat. Commun.* **8,** (2017).
10. Wu, J., Zhang, Z., Tong, C., Li, D., Mei, A., Rong, Y., Zhou, Y., Han, H. & Hu, Y. Two-Stage Melt Processing of Phase-Pure Selenium for Printable Triple-Mesoscopic Solar Cells. *ACS Appl. Mater. Interfaces* **11,** 33879–33885 (2019).
11. Hadar, I., Song, T. Bin, Ke, W. & Kanatzidis, M. G. Modern Processing and Insights on Selenium Solar Cells: The World's First Photovoltaic Device. *Adv. Energy Mater.* **9,** 1–9 (2019).
12. Liu, W., Said, A. A., Fan, W. J. & Zhang, Q. Inverted Solar Cells with Thermally Evaporated Selenium as an Active Layer. *ACS Appl. Energy Mater.* **3,** 7345–7352 (2020).
13. Nielsen, R., Youngman, T. H., Crovetto, A., Hansen, O., Chorkendorff, I. & Vesborg, P. C. K. Selenium Thin-Film Solar Cells with Cadmium Sulfide as a Heterojunction Partner. *ACS Appl. Energy Mater.* **4,** 10697–10702 (2021).
14. Youngman, T. H., Nielsen, R., Crovetto, A., Seger, B., Hansen, O., Chorkendorff, I. & Vesborg, P. C. K. Semitransparent Selenium Solar Cells as a Top Cell for Tandem Photovoltaics. *Sol. RRL* **5,** 1–5 (2021).
15. Silva, L. A. & Cutler, M. Optical properties of liquid Se-Te alloys. *Phys. Rev. B* **42,** 7103–7113 (1990).
16. Tripathi, K., Bahishti, A. A., Majeed Khan, M. A., Husain, M. & Zulfequar, M. Optical properties of selenium–tellurium nanostructured thin film grown by thermal evaporation. *Phys. B Condens. Matter* **404,** 2134–2137 (2009).
17. Reddy, K. V. & Bhatnagar, A. K. Electrical and optical studies on amorphous Se-Te alloys. *J. Phys. D Appl. Phys*

25, 1810–1816 (1992).
18. Hadar, I., Hu, X., Luo, Z. Z., Dravid, V. P. & Kanatzidis, M. G. Nonlinear Band Gap Tunability in Selenium-Tellurium Alloys and Its Utilization in Solar Cells. *ACS Energy Lett.* **4,** 2137–2143 (2019).
19. Ito, S., Kitagawa, N., Shibahara, T. & Nishino, H. Electrochemical Deposition of Te and Se on Flat TiO_2 for Solar Cell Application. *Int. J. Photoenergy* **2014,** 1–5 (2014).
20. McCarthy, C. L. & Brutchey, R. L. Solution processing of chalcogenide materials using thiol–amine "alkahest" solvent systems. *Chem. Commun.* **53,** 4888–4902 (2017).
21. Walker, B. C. & Agrawal, R. Contamination-free solutions of selenium in amines for nanoparticle synthesis. *Chem. Commun.* **50,** 8331 (2014).
22. Zhang, R., Szczepaniak, S. M., Carter, N. J., Handwerker, C. A. & Agrawal, R. A Versatile Solution Route to Efficient $Cu_2ZnSn(S,Se)_4$ Thin-Film Solar Cells. *Chem. Mater.* **27,** 2114–2120 (2015).
23. Miskin, C. K., Deshmukh, S. D., Vasiraju, V., Bock, K., Mittal, G., Dubois-Camacho, A., Vaddiraju, S. & Agrawal, R. Lead Chalcogenide Nanoparticles and Their Size-Controlled Self-Assemblies for Thermoelectric and Photovoltaic Applications. *ACS Appl. Nano Mater.* **2,** 1242–1252 (2019).
24. Deshmukh, S. D., Ellis, R. G., Sutandar, D. S., Rokke, D. J. & Agrawal, R. Versatile Colloidal Syntheses of Metal Chalcogenide Nanoparticles from Elemental Precursors Using Amine-Thiol Chemistry. *Chem. Mater.* **31,** 9087–9097 (2019).
25. Deshmukh, S. D., Weideman, K. G., Miskin, C. K., Kisslinger, K. & Agrawal, R. Solution Phase Growth and Ion Exchange in Microassemblies of Lead Chalcogenide Nanoparticles. *ACS Omega* **6,** 21350–21358 (2021).
26. Deshmukh, S. D., Easterling, L. F., Manheim, J. M., LiBretto, N. J., Weideman, K. G., Miller, J. T., Kenttämaa, H. I. & Agrawal, R. Analyzing and Tuning the Chalcogen–Amine–Thiol Complexes for Tailoring of Chalcogenide Syntheses. *Inorg. Chem.* **59,** 8240–8250 (2020).
27. Zhao, X., Deshmukh, S. D., Rokke, D. J., Zhang, G., Wu, Z., Miller, J. T. & Agrawal, R. Investigating Chemistry of Metal Dissolution in Amine–Thiol Mixtures and Exploiting It toward Benign Ink Formulation for Metal Chalcogenide Thin Films. *Chem. Mater.* **31,** 5674–5682 (2019).
28. Murria, P., Miskin, C. K., Boyne, R., Cain, L. T., Yerabolu, R., Zhang, R., Wegener, E. C., Miller, J. T., Kenttämaa, H. I. & Agrawal, R. Speciation of CuCl and $CuCl_2$ Thiol-Amine Solutions and Characterization of Resulting Films: Implications for Semiconductor Device Fabrication. *Inorg. Chem.* **56,** 14396–14407 (2017).
29. Tverjanovich, A., Cuisset, A., Fontanari, D. & Bychkov, E. Structure of Se–Te glasses by Raman spectroscopy and DFT modeling. *J. Am. Ceram. Soc.* **101,** 5188–5197 (2018).
30. Lucovsky, G., Mooradian, A., Taylor, W., Wright, G. B. & Keezer, R. C. Identification of the Fundamental Vibrational Modes Of Trigonal, Monoclinic and Amorphous Selenium. *Solid State Commun.* **5,** 113–117 (1967).
31. Brodsky, M. H., Gambino, R. J., Smith, J. E. & Yacoby, Y. The Raman Spectrum of Amorphous Tellurium. *Phys. Status Solidi* **52,** 609–614 (1972).
32. Singh, S. C., Mishra, S. K., Srivastava, R. K. & Gopal, R. Optical properties of selenium quantum dots produced with laser irradiation of water suspended Se nanoparticles. *J. Phys. Chem. C* **114,** 17374–17384 (2010).
33. Liu, R. & Xu, K. Solvent engineering for perovskite solar cells: A review. *Micro Nano Lett.* **15,** 349–353 (2020).
34. Salah, N., Habib, S. S. & Khan, Z. H. Direct bandgap materials based on the thin films of Se_xTe_{100-x} nanoparticles. *Nanoscale Res. Lett.* **7,** 509 (2012).

Table of Content Graphic: